RESEARCH ARTICLE

WILEY

Self-powered wireless body area network for multi-joint movements monitoring based on contact-separation direct current triboelectric nanogenerators

Feng Liu[1,2,3] | Yuan Feng[2,3] | Youchao Qi[2,4] | Guoxu Liu[2] | Han Zhou[2] | Yuan Lin[2] | Beibei Fan[2,3] | Zhi Zhang[2,4] | Sicheng Dong[2,4] | Chi Zhang[1,2,3,4] [ID]

[1]School of Mechanical Engineering, Guangxi University, Nanning, the People's Republic of China

[2]CAS Center for Excellence in Nanoscience, Beijing Key Laboratory of Micro-nano Energy and Sensor, Beijing Institute of Nanoenergy and Nanosystems, Chinese Academy of Sciences, Beijing, the People's Republic of China

[3]Center on Nanoenergy Research, School of Physical Science and Technology, Guangxi University, Nanning, the People's Republic of China

[4]School of Nanoscience and Technology, University of Chinese Academy of Sciences, Beijing, the People's Republic of China

Correspondence
Chi Zhang, CAS Center for Excellence in Nanoscience, Beijing Key Laboratory of Micro-nano Energy and Sensor, Beijing Institute of Nanoenergy and Nanosystems, Chinese Academy of Sciences, Beijing 100083, the People's Republic of China.
Email: czhang@binn.cas.cn

Abstract

Body area network has attracted extensive attention for its applications in athletics, medical, diagnosis, and rehabilitation training in the next generation personalized health care solutions. Here, a contact-separation direct current triboelectric nanogenerators (CSDC-TENGs) based self-powered wireless body area network (SWBAN) is reported that enables multi-joint movements monitoring for human motion. The CSDC-TENG is designed as a flexible active sensor with an internal contact switch, and the flexible substrate makes the TENG-sensor stick onto skin easily. Due to the internal switch, the CSDC-TENG could generate a DC current, a large instantaneous output voltage exceeds 700 V, and an instantaneous power can reach 1.076 W, which is more than 23 000 times higher than that of the traditional contact-separation mode TENG in same size and materials without the switch. By coupling with flexible coil, the fixed high-frequency radio signals can be modulated and emitted clearly ranging from 6 to 16 MHz, which can be wirelessly received and demodulated through a reader. Moreover, the SWBAN is demonstrated in a real time monitoring system for joints motion. This work has realized the wearable TENG for self-powered wireless real-time monitoring of body movements driven by low-frequency human daily activities, which may promote a tremendous development of intelligent healthcare, wireless sensing system and body area network.

KEYWORDS

body area network, flexible electronics, radio frequency identification, self-powered wireless sensing system, triboelectric nanogenerator

1 | INTRODUCTION

With the development of wearable devices, electronic, and information technology, body area network is expected to be used for a range of applications of sports training, healthcare monitoring, and remote diagnosis.[1–7] By integrating biosensors and wearable electronics onto human body seamlessly, these devices will be merge with bodies to extend various perceptions.[8–14] Body area healthcare monitoring platforms have recently emerged, including applications of physiological fitness tracking, body condition monitoring, and clinical diagnostics.[15–30] However, direct wiring connections between sensor nodes on the human body interfere in physical activities, wireless technologies require each sensor node to be powered separately for long-term operation, and bluetooth/Wifi-based devices raise privacy and data security concerns.[1,11,31–33] Therefore, there is a highly desire for body area network without the external power to achieve body movements monitoring.

Triboelectric nanogenerator (TENG) as a newly energy technology based on the conjugation effects of contact electrification and electrostatic induction emerging in recent years, which could convert a variety of environmental mechanical energy and human kinetic energy into electrical outputs.[34–44] Various TENG-based self-powered sensing devices have been developed, such as human physiological signal monitoring platform,[17,24,45–47] wireless sensing system,[28,48–50] and so on. In addition, due to the high detection sensitivity and large electrical output signal, the TENG have been used for human real-time monitoring of breathing, heart rate, finger touch, joint movement, and walking.[51–55] These research efforts have shown the enormous potential of the TENG as a battery-free sensor system, which is a very promising solution to achieve the self-powered wireless body area network.

In this work, a self-powered wireless body area network is demonstrated by contact-separation direct current triboelectric nanogenerators (CSDC-TENGs) and flexible coils. The CSDC-TENG is designed as an active sensor consisting of poly-tetrafluoroethylene (PTFE), copper, and flexible polyethylene terephthalate (PET) substrate with an internal contact switch. The peak open-circuit voltage value of CSDC-TENG can reach up to 736 V, short-circuit current is 10.6 μA, peak power is 1.076 W (4.2 kW m^{-2}), and impedance is 200 kΩ. Compared to the traditional contact-separation mode TENG in same size and materials without the switch, the voltage and peak power are improved approximately 10 and 24 000 times, respectively. The RF signals with the fixed frequency ranging from 6 to 16 MHz can be modulated and transmitted by the coupled emitter composed of CSDC-TENG and flexible coil, basically without electric energy loss, which can be wirelessly received and demodulated by the reader. With a flexible relay network, signals from multiple emitter nodes can be converged, and received by the same receiver. Furthermore, the SWBAN is demonstrated in real time body movements monitoring system for multi-joint movements. This work has realized a wearable TENG body area network for body movements monitoring driven by low-frequency human motions, which may have great significance and prospects in wireless communication and self-powered intelligent sensor networks.

2 | RESULTS AND DISCUSSION

2.1 | Self-powered wireless body area network system

The schematic illustration of self-powered wireless body area network (SWBAN) system is shown in Figure 1A, which is performing continuous body joints movements and displaying real-time data on a smart phone via wireless transmission. The SWBAN driven by low-frequency human body movements consists of contact-separation direct current triboelectric nanogenerator (CSDC-TENG) based emitters, a flexible coil based relay network, and a reader system, as shown in Figure 1B. The CSDC-TENG harvests the human motion energy and converts it into DC pulse output, which is then converted into RF signals with fixed frequency by the CSDC-TENG based emitter. Then the signals from multiple emitter nodes can be received and converged by the flexible relay network. Finally, the reader system, which includes a flexible coil and a processing system that runs on a PC, is used for receiving and demodulating signals from the hub of the relay network. The signals with different frequencies captured by the reader system can be matched to the corresponding nodes, and the measured data for human motion could be sent out to the various terminals.

The equivalent circuit diagram of the SWBAN system is shown in Figure 1C, including several emitter nodes, a relay network and a reader system. Theoretical analysis has shown that the traditional contact-separation mode TENG can be considered as a voltage source connected in series with a capacitor.[56–58] Thus, the electrification model of CSDC-TENG can be seen as a voltage source (V_{TENG}), a capacitor (C_{TENG}) and a switch connected in series. By coupling with a flexible coil, the integrated emitter electrification model can be seen as an LC resonant circuit that includes a voltage source and a switch. When the CSDC-TENG is triggered by a slight external stimulus, the internal switch closes and a pulsed voltage
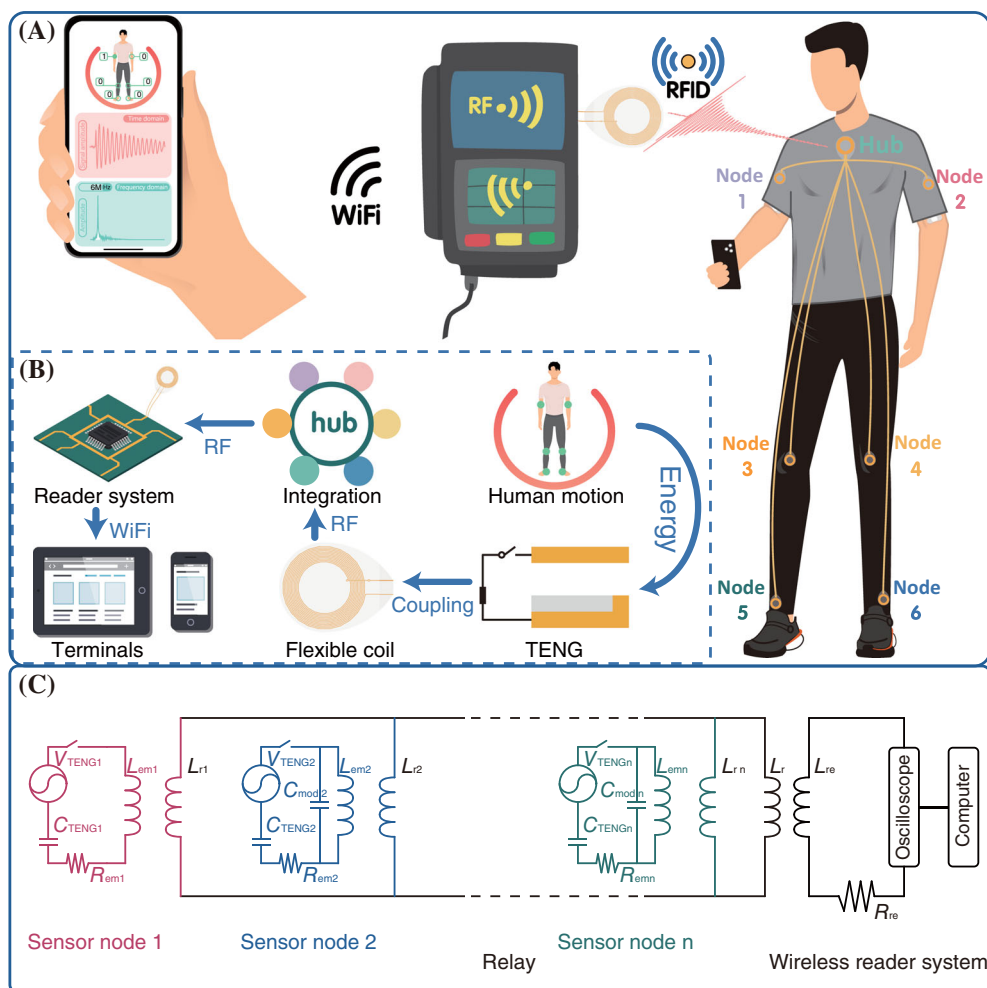
FIGURE 1 Self-powered wireless body area network system. (A,B) System diagram of the contact-separation direct current triboelectric nanogenerator based body area network by human motion energy for joints monitoring and wireless communication. (C) Equivalent circuit diagram of the self-powered wireless body area network (SWBAN) system.

output will be generated. Then the voltage output would be coupled to the LC circuit to produce a fixed frequency resonant signal. The resonant signals are transmitted from each emitter node, and then converged by the flexible coil based relay network. Finally, the reader system analyzes the signals received from the hub of the relay network, and obtains the resonant frequency of the signals by the Fast Fourier Transform (FFT) algorithm.

2.2 | Schematic and characterization of CSDC-TENG

The structure of the CSDC-TENG is shown in Figure 2A–C and Figure S1E. Copper and PTFE were selected as the two triboelectric materials for effective triboelectrification because of their strong abilities to lose and attract electrons, respectively. Similar to the traditional TENG, the copper film acts as both positive triboelectric material and

electrode, while the PTFE film with copper pasted on its backside act as the negative triboelectric material and electrode. Different from traditional structures, the positive and the negative copper electrodes each extend a contact point that constitutes the internal switch. In detail, the copper film was pasted on a PET substrate, covering triboelectrification area and the contact point. Notably, the copper film is integral and both the front and back of the contact points are covered (Figure S1E[i]). On the other hand, the PTFE film with copper electrode was adhered to another PET substrate with three sides wrap-around PET support (Figure S1E[ii]). It is worth noting that the PET substrate and the PET support are molded in one piece, which provides good flexibility for substrate and decent strength for support. The copper electrode on the back of the PTFE extended to the bottom of the PET support and serves as a contact point for internal charge exchange. On the opposite side, there was another contact point that outputs electricity to external circuit through a wire. By the way, the other
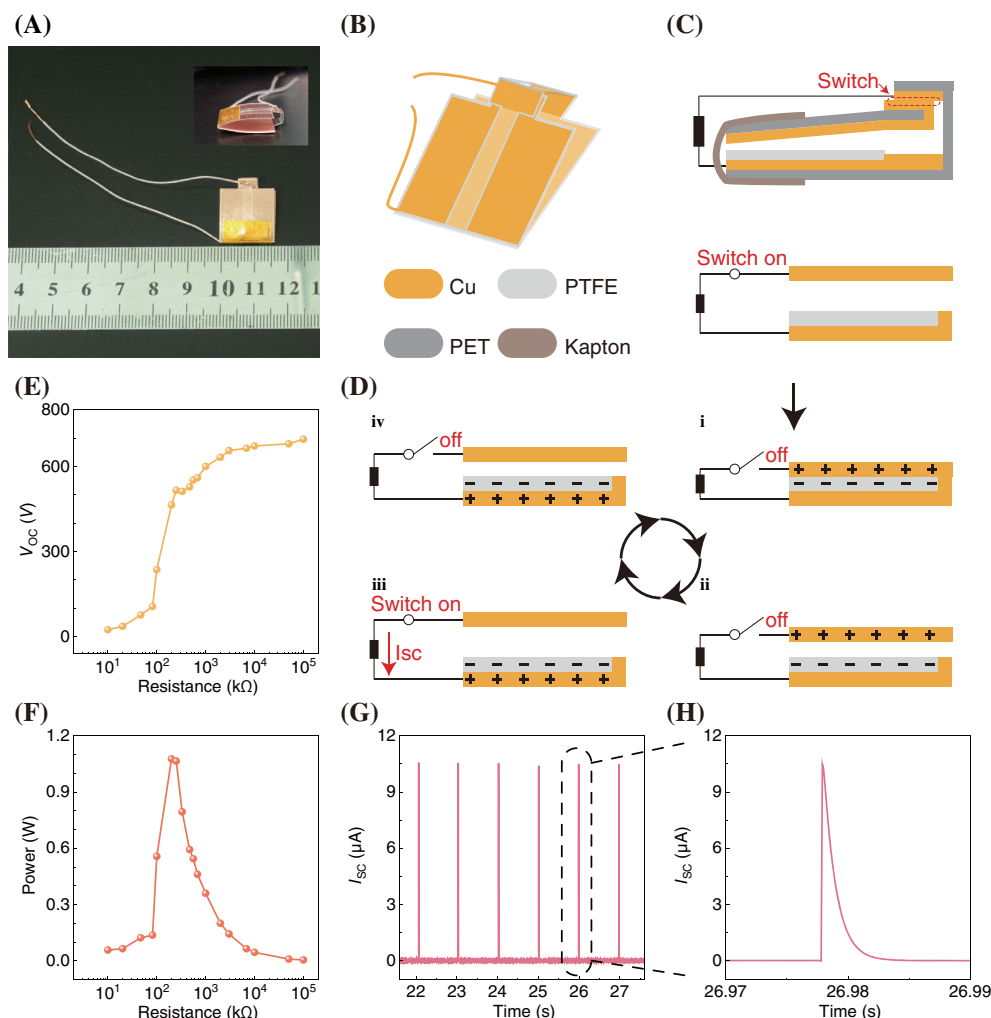
FIGURE 2 Working mechanism and output performance of the contact-separation direct current triboelectric nanogenerator (CSDC-TENG). (A) The photographic image of CSDC-TENG. (B,C) Structure of the designed CSDC-TENG. (D) Working mechanism of CSDC-TENG. Peak voltage value (E) and the instantaneous power (F) of CSDC–TENG under different impedances. (G,H) Short-circuit current output of CSDC-TENG under cyclic pressing.

wire for the external circuit was connected to the copper electrode of the PTFE. Kapton film has the advantages of strong flexibility and high elasticity modulus, which was used as a spring wrapping the two layers to ensure the contact and separation of the two triboelectric layers. The gap between the two contact points of the three-sided wrap-around PET support is 3 mm. Detailed information on physical dimensions and manufacturing methods can be found in Section 4.

The working mechanism illustration of the CSDC-TENG is shown in Figure 2D and Figure S1A. First, with the external excitation applied to the CSDC-TENG, the copper triboelectric layer and the PTFE triboelectric layer are fully contacted. Because of the different electronegativity, the two triboelectric layers obtain equal positive and negative charges, respectively (Figure 2D[i], Figure S1A[i]). In this stage, the switch is off and no electricity is output to the external circuit. When the

excitation is removed in the next stage (Figure 2D[ii], Figure S1A[ii]), the two triboelectric layers start to separate under the elastic force of the Kapton film and the two electrodes generated an electric potential difference due to electrostatic induction. However, the switch remains off and there is still no electricity output to the external circuit. When the two triboelectric layers are completely separated in the third stage (Figure 2D[iii], Figure S1A[iii]), the contact point of the copper triboelectric layer is in contact with the point on the top of the PET support and the switch is turned on. An instantaneous electricity is output to the external circuit once. Similar to the second stage, the two triboelectric layers are separated again and no electricity output to the external circuit as the switch is off (Figure 2D[iv], Figure S1A [iv]). In subsequent cycles, besides the triboelectrification and electrostatic induction, an extra internal charges exchange occurs when the two triboelectric layers are in

fully contact, as shown in Figure S1F. The electrons flow from the electrode of PTFE triboelectric layer to the copper triboelectric layer through the contact points of the two triboelectric layer electrodes, which is different from the first working process.

Owing to the ingenious design, CSDC-TENG is able to generate DC current. To gain an intuitive understanding of the output performance of the CSDC-TENG, a linear motor with a displacement of 3 mm was used to control the contact separation motion, which is shown in Figure S2. When a force of 10 N was applied to the CSDC-TENG with a frequency of 1 Hz, the DC pulsed electrical output with the motion was observed (Figure 2G). The peak open-circuit voltage value can reach up to 736 V, and the peak short-circuit current is 10.6 μA, as shown in Figure S1B,C and Figure 2G,H. Figure 2E shows the peak voltage under different external load resistances in the range of 10 kΩ to 100 MΩ. As shown in Figure 2F, the matched impedance is 200 kΩ, and the peak power density of the CSDC-TENG is 4.203 kW m^{-2} (1.076 W in a working area of 2.56 cm^2), where the power was calculated by $P = U^2/R$. Compared to the traditional contact-separation mode TENG in same size and materials without the switch, the voltage and peak power are improved 10 and 23 900 times, respectively (Refer to Figure S4, for detailed data of traditional TENG output without the switch). In addition, the CSDC-TENG was characterized at different contact frequencies (Figure S3 and Video S1). The results show that the output is stable and slightly decreases with increasing contact frequency, which is different from the traditional TENG (Figure S5). The explanation here is that the contact conditions between the two triboelectric layers is not so good due to the accelerated contact frequency. This means that the charge at the interface of the two triboelectric layers has been transferred sufficiently because of the internal switch. While the TENG can achieve DC output through external power management circuit,[59] spark switches,[60] and travel switches with diode,[61] these methods require extra parts and all resulting in incomplete utilization or loss of electric power. In particular, the CSDC-TENG does not require external components or circuits and has no electric energy loss in the output of DC current.

2.3 | Performance of the wireless transmission

The instantaneous discharge generated by the internal switch not only outputs DC current and enhances the output performance, but also converts low-frequency input motion signals into high-frequency electromagnetic wave signals. Due to the inherent capacitive property of CSDC-TENG, an LC resonant circuit can be formed by coupling with an inductance coil. A large electricity can be instantaneously output because of the voltage source property and the internal switch of CSDC-TENG. In theory, the instantaneous electricity output will oscillate in the LC resonant circuit and be converted into high-frequency electromagnetic wave signal, which can be wirelessly transmitted by the inductance coil. It should be noted that the CSDC-TENG outputs electricity only once in a complete working cycle, avoiding false triggering and the repeated acquisition of signals. Thus, a flexible coil was designed for consisting the emitter and transmitting radio signal, as shown in the inset of Figure 3A. Detailed information on the design dimensions and manufacturing method can be found in Figure S6 and Section 4. The resonant frequency (f) of the coupled emitter signal transmitted by the LC circuit can be calculated by Equation (1), which is determined by the capacitance of the CSDC-TENG (C_{TENG}) and the impedance of the flexible coil (L_{em}). The emitter capacitance (C_{TENG}) and inductance (L_{em}) can be measured as 16.5 pF and 6 μH, respectively. The fundamental frequency can be calculated as 16 MHz.

$$f = \frac{1}{2\pi\sqrt{L_{em}C_{TENG}}} \tag{1}$$

According to Equation (1), the resonant frequency can be modulated by changing the capacitance or inductance. Therefore, the modulation capacitor (C_{mod}) is introduced and coupled in parallel to the emitter for signal frequency modulation. The coupled emitter works as a wireless sensor node, and its electrification model is shown in Figure 3B. The emit frequency (f_{em}) is determined by the emitter inductance (L_{em}) and emitter capacitance (C_{TENG} plus C_{mod}), which can be expressed by

$$f_{em} = \frac{1}{2\pi\sqrt{L_{em}(C_{TENG} + C_{mod})}} \tag{2}$$

In order to verify the principle and characterization, a series of single point transmit-receive experiments were performed with detailed description and analysis (Figure S7 and Video S2). After the results had been verified well, the relay was introduced for a series of experiments, as shown in Figure 3. The schematic diagram of the experimental emitter and receiver system with relay is shown in Figure 3A, and the experimental equivalent circuit is shown in Figure 3B. RF signals are generated and transmitted by the coupled emitter, finally received and demodulated by the flexible coil based reader. As shown in Figure 3C, the oscillating signal that generates
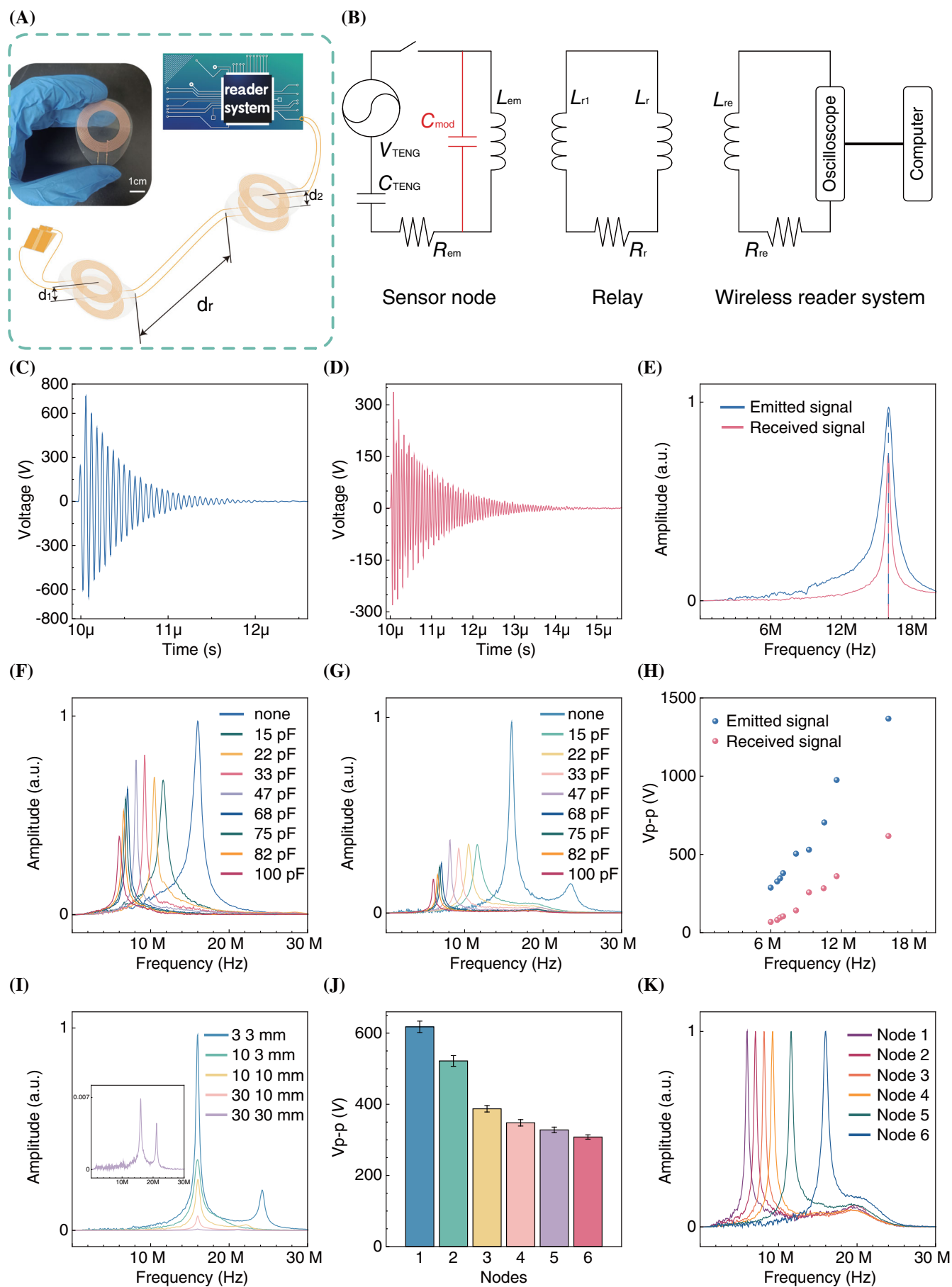
FIGURE 3 Legend on next page.

amplitude decay has a unidirectional maximum value of more than 700 V. Received signal of the flexible coil based reader system is shown in Figure 3D. The distance between the emitting coil and relay (d_1) is 3 mm, the length of the relay is 60 cm, and the distance between the receiving coil and relay (d_2) is 3 mm. The maximum peak–peak value of the received resonant signal is approximately 600 V, which is easy to detected and identify. Figure 3E shows the normalized FFT spectrum corresponding to the emitted signal (Figure 3C) and the received signal (Figure 3D). The frequency domain signals are clearly identifiable and they have the same characteristic frequency value at 16 MHz. By changing the value of the modulation capacitor, the emitter frequency can be tuned in the range of 6–16 MHz, as shown in Figure 3F. The normalized FFT spectrum of the emitted signal shows that the signal can be effectively modulated with a clear frequency span of at different capacitance values. Figure 3G shows the normalized FFT spectrum corresponding to the signals received by the reader system, and their characteristic frequency are same as the emitted signals at the corresponding capacitance values. Figure 3H shows the maximum peak–peak value of the emitted and received resonant signals at different frequency. Even though the value decreases as the frequency decreases, the emitted resonant signals remain at hundreds to thousand volts and the received resonant signals can reach tens to hundreds of volts (Figure S9 and Figure S10). As shown in Figure 3I, the wireless transmission capability is verified by changing the distances d_1 and d_2. The normalized FFT spectrum of the received signals shows the well consistency with increasing distances, verifying the stability of the signal at variable distances. In addition, the relay can be connected in parallel with flexible coils to increase the nodes. The received signal of the reader decreases with the increase of nodes, however, it still in the hundreds of volts range (Figure 3J, the experiments here were performed at 16 MHz of the emitted signal, since the signal value is maximum.). Six different signals in the frequency range of 6–16 MHz were selected for application demonstrations, which can be easily distinguished. The normalized FFT spectrum of the six chosen signals is shown in Figure 3K.

2.4 | Self-powered wireless body area network for body movements monitoring

Furthermore, the SWBAN is demonstrated in real-time monitoring of multi-joints motion. As a concept demonstration, six joint nodes were selected at the elbows, legs, and foots for body movements detection, and the number of sensor nodes can be readily increased or decreased depending on the required application. Figure 4A depicts the signal transmission process of the monitoring system, including a smart phone, the reader, and the network on body. The six joint nodes of the body generate signals with corresponding joint movements, which can be pooled at the hub of the relay network and then transmitted to the reader. The data processed by the reader system can be sent to the smartphone via WiFi. To accurately read the human motion statuses, the demodulator program of the reader system converts the resonant signals into frequency domain signals and matches to the corresponding nodes. Specifically, the RF signals are acquired by the reader coil, then denoised by the filter, and the FFT module is used for time-frequency conversion. Finally, the characteristic frequencies are obtained by the peak detection module and matched to the corresponding node (Figure 4B). Figure 4C shows the relay network with a hub and six nodes on the cloth, and the illustration of the coupled emitter on body joints (such as elbow) is shown in Figure 4D. To show the potential of SWBAN in the field of human motion monitoring, a demonstration interface was designed to visualize the movements of different body joints (Figures 1A and 4E). In the mobile interface, all collected data, including time domain waves, frequency domain signals, and the motion status and counts of the corresponding joints, can be displayed simultaneously in real time. Figure 4F presents continuous body movements of bending elbows, lifting legs and stepping with corresponding data records (refer to Figure S8 and Video S3, for the motion demonstration. The output of CSDC-TENG with different joint movements is shown in Figure S11). Different signals accurately correspond to different joint movements, which shows the capability of the SWBAN to perform multi-nodes, continuous and wireless monitoring for human activities.

FIGURE 3 Wireless signals characterization of the CSDC-TENG coupled flexible coil with relay. (A) System diagram of the experimental emitter and receiver with relay. (B) Circuit diagram of the experiment system. (C) Emitted signal of the CSDC-TENG coupled flexible coil emitter. (D) Received signal of the flexible coil based receiver. (E) Frequency spectrum of (C) and (D) after FFT. Frequency domain signals of the coupled emitter (F) and receiver (G) with the modulation capacitance changing. (H) Peak-to-peak voltage value of the time domain signals corresponds to (F) and (G). (I) Frequency spectrum amplitudes at different distances between the emitted coil and relay (d_1) and the received coil and relay (d_2). (J) Peak-to-peak voltage values of the received signal (time domain) from 1 to 6 nodes. (K) Normalized frequency spectrum of six selected signals for application.
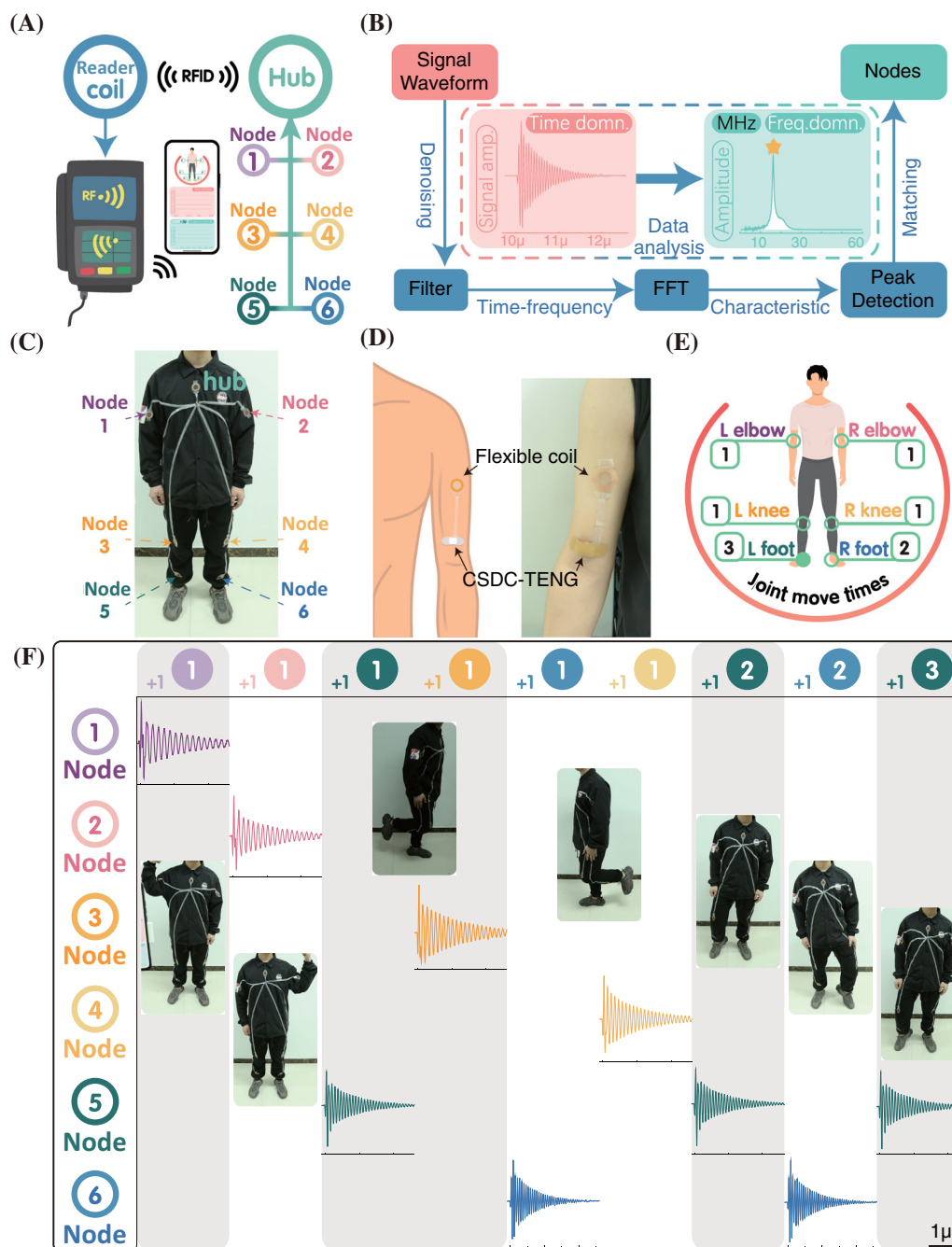
FIGURE 4 Self-powered wireless body area network for multi-joint movements monitoring. (A) Schematic diagram of the SWBAN monitoring system. (B) Signal processing schematic diagram of the monitoring system. (C) Demonstration of the relay network on the cloth. (D) Demonstration of the CSDC-TENG coupled flexible coil emitter on body. (E) The monitoring system interface shows the number of movements of each joint. (F) Motion data recording.

3 | CONCLUSION

In summary, a self-powered wireless body area network based on CSDC-TENGs was reported. As a flexible active sensor for low-frequency stimuli detection, the CSDC-TENG can generate DC with excellent performance of the peak open-circuit voltage exceeds 700 V, peak power density reaches 4.2 kW m^{-2}, and impedance is 200 kΩ.

Compared to the traditional contact-separation mode TENG in the same size and materials without the internal switch, the peak power density is improved 23 900 times. By coupling with the designed flexible coil and the modulation capacitor, the fixed high-frequency radio signals can be emitted clearly ranging from 6 to 16 MHz, which can be wirelessly received and demodulated by the reader system. With a flexible relay network, signals from

multiple emitter nodes can be pooled, and then received by the same receiver. Moreover, the SWBAN was demonstrated in a real time monitoring system for multi-joint movements. There is no rigid components or complex chips on body, which improves wearing comfort compared to traditional designs of Bluetooth or NFC. This study provides a way of sensing and monitoring human activities by low-frequency joints motion without external power supply, which can be utilized in athletics, daily routines, and remote diagnosis to facilitate real-time monitoring and personalized healthcare.

4 | EXPERIMENTAL SECTION

4.1 | Fabrication of the CSDC-TENG

CSDC-TENG is composed of two triboelectric layers, both based on flexible PET substrate (100 μm in thickness). A laser fast scanning and cutting machine (D90M) was used to cut PET sheets into a square shape (the sides of the square are 16 mm) with a convex part (contact point), and another square shape with a rectangle strap. An integral copper film (65 μm thick) was adhered to the square PET sheet with a convex part, covering triboelectrification area (16 × 16 mm) and both front and back sides of the convex part (contact point). Then the rectangle strap of the PET sheet was fold into a cubic structure surrounded on three sides for support. Another copper film (65 μm thick) and PTFE film (50 μm thick) were sequentially attached to the square PET sheet with rectangle strap, covering triboelectrification area and extending a contact point. The PTFE film had not been surface-modified or polarized. As for the contact point of external circuit, it is on the opposite side. The other wire for the external circuit was connected to the electrode of PTFE.

4.2 | Fabrication of the flexible coil

The flexible coils were manufactured using commercial FPCB processes. The substrate material is PET (18 μm thick), packaged on both sides. The Cu coil in the middle is 35 μm thick.

4.3 | Measurement and characterization

The linear motor (MBT-37 × 120/280 × 360-C-SYS-SP-01) was used to drive the CSDC-TENG to control the contact separation motion. The open-circuit voltage and short-circuit current of the CSDC-TENG were measured by an oscilloscope (MDO3024 Tektronix) and an electrometer (Keithley 6514), respectively. The oscilloscope (MDO3024 Tektronix) with a high-voltage probe (P6015A Tektronix) was used to measure the oscillating signals.

4.4 | Reader system

The reader system consists of a flexible coil, an oscilloscope (MDO3024; Tektronix) with a high-voltage probe (P6015A; Tektronix), and an independently developed LabVIEW program.

CONFLICT OF INTEREST STATEMENT
The authors declare no conflict of interest.

ORCID
Chi Zhang https://orcid.org/0000-0002-7511-805X

REFERENCES
1. Chu B, Burnett W, Chung JW, Bao Z. Bring on the bodyNET. *Nature*. 2017;549(7672):328-330.
2. Gao W, Emaminejad S, Nyein HYY, et al. Fully integrated wearable sensor arrays for multiplexed in situ perspiration analysis. *Nature*. 2016;529(7587):509-514.
3. Son D, Lee J, Qiao S, et al. Multifunctional wearable devices for diagnosis and therapy of movement disorders. *Nat Nanotechnol*. 2014;9(5):397-404.
4. Sreenilayam SP, Ahad IU, Nicolosi V, Acinas Garzon V, Brabazon D. Advanced materials of printed wearables for physiological parameter monitoring. *Mater Today*. 2020;32: 147-177.

5. Tee BCK, Chortos A, Berndt A, et al. A skin-inspired organic digital mechanoreceptor. *Science*. 2015;350(6258):313-316.

6. Yamamoto Y, Harada S, Yamamoto D, et al. Printed multifunctional flexible device with an integrated motion sensor for health care monitoring. *Sci Adv*. 2016;2(11):e1601473.

7. Yang Y, Gao W. Wearable and flexible electronics for continuous molecular monitoring. *Chem Soc Rev*. 2019;48(6):1465-1491.

8. Han S, Kim J, Won SM, et al. Battery-free, wireless sensors for full-body pressure and temperature mapping. *Sci Transl Med*. 2018;10(435):eaan4950.

9. Kim D-H, Lu N, Ma R, et al. Epidermal electronics. *Science*. 2011;333(6044):838-843.

10. Kim J, Salvatore GA, Araki H, et al. Battery-free, stretchable optoelectronic systems for wireless optical characterization of the skin. *Sci Adv*. 2016;2(8):e1600418.

11. Someya T, Bao Z, Malliaras GG. The rise of plastic bioelectronics. *Nature*. 2016;540(7633):379-385.

12. Tee BCK, Chortos A, Dunn RR, Schwartz G, Eason E, Bao Z. Tunable flexible pressure sensors using microstructured elastomer geometries for intuitive electronics. *Adv Funct Mater*. 2014;24(34):5427-5434.

13. Wang C, Hwang D, Yu Z, et al. User-interactive electronic skin for instantaneous pressure visualization. *Nat Mater*. 2013;12(10):899-904.

14. Xu S, Zhang Y, Jia L, et al. Soft microfluidic assemblies of sensors, circuits, and radios for the skin. *Science*. 2014;344(6179):70-74.

15. Chung HU, Kim BH, Lee JY, et al. Binodal, wireless epidermal electronic systems with in-sensor analytics for neonatal intensive care. *Science*. 2019;363(6430):eaau0780.

16. Dautta M, Jimenez A, Dia KKH, Rashid N, Faruque MAA, Tseng P. Wireless Qi-powered, multinodal and multisensory body area network for mobile health. *IEEE Internet Things J*. 2021;8(9):7600-7609.

17. Fang Y, Zou Y, Xu J, et al. Ambulatory cardiovascular monitoring via a machine-learning-assisted textile triboelectric sensor. *Adv Mater*. 2021;33(41):2104178.

18. Hajiaghajani A, Afandizadeh Zargari AH, Dautta M, Jimenez A, Kurdahi F, Tseng P. Textile-integrated metamaterials for near-field multibody area networks. *Nat Electron*. 2021;4(11):808-817.

19. Kim Y, Suh JM, Shin J, et al. Chip-less wireless electronic skins by remote epitaxial freestanding compound semiconductors. *Science*. 2022;377(6608):859-864.

20. Lee Y, Chung JW, Lee GH, et al. Standalone real-time health monitoring patch based on a stretchable organic optoelectronic system. *Sci Adv*. 2021;7(23):eabg9180.

21. Li J, Dong Y, Park JH, Yoo J. Body-coupled power transmission and energy harvesting. *Nat Electron*. 2021;4(7):530-538.

22. Lin R, Kim H-J, Achavananthadith S, et al. Wireless battery-free body sensor networks using near-field-enabled clothing. *Nat Commun*. 2020;11(1):444.

23. Liu X, Wang Y, Wang G, et al. An ultrasound-driven implantable wireless energy harvesting system using a triboelectric transducer. *Matter*. 2022;5(12):4315-4331.

24. Meng K, Zhao S, Zhou Y, et al. A wireless textile-based sensor system for self-powered personalized health care. *Matter*. 2020;2(4):896-907.

25. Niu S, Matsuhisa N, Beker L, et al. A wireless body area sensor network based on stretchable passive tags. *Nat Electron*. 2019;2(8):361-368.

26. Tian L, Zimmerman B, Akhtar A, et al. Large-area MRI-compatible epidermal electronic interfaces for prosthetic control and cognitive monitoring. *Nat Biomed Eng*. 2019;3(3):194-205.

27. Tian X, Lee PM, Tan YJ, et al. Wireless body sensor networks based on metamaterial textiles. *Nat Electron*. 2019;2(6):243-251.

28. Wang H, Wang J, Yao K, et al. A paradigm shift fully self-powered long-distance wireless sensing solution enabled by discharge-induced displacement current. *Sci Adv*. 2021;7(39):eabi6751.

29. Zhang N, Huang F, Zhao S, et al. Photo-rechargeable fabrics as sustainable and robust power sources for wearable bioelectronics. *Matter*. 2020;2(5):1260-1269.

30. Zhang Q, Xin C, Shen F, et al. Human body IoT systems based on the triboelectrification effect: energy harvesting, sensing, interfacing and communication. *Energ Environ Sci*. 2022;15(9):3688-3721.

31. Al Ameen M, Liu J, Kwak K. Security and privacy issues in wireless sensor networks for healthcare applications. *J Med Syst*. 2012;36(1):93-101.

32. Cao H, Leung V, Chow C, Chan H. Enabling technologies for wireless body area networks: a survey and outlook. *IEEE Commun Mag*. 2009;47(12):84-93.

33. Kim J, Campbell AS, de Ávila BE-F, Wang J. Wearable biosensors for healthcare monitoring. *Nat Biotechnol*. 2019;37(4):389-406.

34. Fan F-R, Tian Z-Q, Lin WZ. Flexible triboelectric generator. *Nano Energy*. 2012;1(2):328-334.

35. Wang S, Lin L, Wang ZL. Nanoscale triboelectric-effect-enabled energy conversion for sustainably powering portable electronics. *Nano Lett*. 2012;12(12):6339-6346.

36. Wang ZL, Wu W. Nanotechnology-enabled energy harvesting for self-powered micro-/Nanosystems. *Angew Chem Int ed*. 2012;51(47):11700-11721.

37. Wang ZL. Triboelectric nanogenerators as new energy technology for self-powered systems and as active mechanical and chemical sensors. *ACS Nano*. 2013;7(11):9533-9557.

38. Wang S, Lin L, Wang ZL. Triboelectric nanogenerators as self-powered active sensors. *Nano Energy*. 2015;11:436-462.

39. Hinchet R, Yoon H-J, Ryu H, et al. Transcutaneous ultrasound energy harvesting using capacitive triboelectric technology. *Science*. 2019;365(6452):491-494.

40. Wang ZL, Wang AC. On the origin of contact-electrification. *Mater Today*. 2019;30:34-51.

41. Song Y, Wang N, Wang Y, Zhang R, Olin H, Yang Y. Direct current triboelectric nanogenerators. *Adv Energy Mater*. 2020;10(45):2002756.

42. Ma C, Kim B, Kim S-W, Park N-G. Dynamic halide perovskite heterojunction generates direct current. *Energ Environ Sci*. 2021;14(1):374-381.

43. Ryu H, Park H-m, Kim M-K, et al. Self-rechargeable cardiac pacemaker system with triboelectric nanogenerators. *Nat Commun*. 2021;12(1):4374.

44. Wang ZL. From contact electrification to triboelectric nanogenerators. *Rep Prog Phys*. 2021;84(9):096502.

45. Ma Y, Zheng Q, Liu Y, et al. Self-powered, one-stop, and multifunctional implantable triboelectric active sensor for real-time biomedical monitoring. *Nano Lett*. 2016;16(10):6042-6051.

46. Zheng Q, Zhang H, Shi B, et al. In vivo self-powered wireless cardiac monitoring via implantable triboelectric nanogenerator. *ACS Nano*. 2016;10(7):6510-6518.

47. Ouyang H, Liu Z, Li N, et al. Symbiotic cardiac pacemaker. *Nat Commun*. 2019;10(1):1821.

48. Wen F, Wang H, He T, et al. Battery-free short-range self-powered wireless sensor network (SS-WSN) using TENG based direct sensory transmission (TDST) mechanism. *Nano Energy*. 2020;67:104266.

49. Zhang C, Chen J, Xuan W, et al. Conjunction of triboelectric nanogenerator with induction coils as wireless power sources and self-powered wireless sensors. *Nat Commun*. 2020;11(1):58.

50. Zhang C, Chen J, Xuan W, et al. Triboelectric nanogenerator-enabled fully self-powered instantaneous wireless sensor systems. *Nano Energy*. 2022;92:106770.

51. Bai P, Zhu G, Jing Q, et al. Membrane-based self-powered triboelectric sensors for pressure change detection and its uses in security surveillance and healthcare monitoring. *Adv Funct Mater*. 2014;24(37):5807-5813.

52. Yang P-K, Lin L, Yi F, et al. A flexible, stretchable and shape-adaptive approach for versatile energy conversion and self-powered biomedical monitoring. *Adv Mater*. 2015;27(25):3817-3824.

53. Yi F, Lin L, Niu S, et al. Stretchable-rubber-based triboelectric nanogenerator and its application as self-powered body motion sensors. *Adv Funct Mater*. 2015;25(24):3688-3696.

54. Yang ZW, Pang Y, Zhang L, et al. Tribotronic transistor Array as an active tactile sensing system. *ACS Nano*. 2016;10(12):10912-10920.

55. Kim M-K, Kim M-S, Kwon H-B, Jo S-E, Kim Y-J. Wearable triboelectric nanogenerator using a plasma-etched PDMS–CNT composite for a physical activity sensor. *RSC Adv*. 2017;7(76):48368-48373.

56. Niu S, Wang S, Lin L, et al. Theoretical study of contact-mode triboelectric nanogenerators as an effective power source. *Energ Environ Sci*. 2013;6(12):3576-3583.

57. Niu S, Zhou YS, Wang S, et al. Simulation method for optimizing the performance of an integrated triboelectric nanogenerator energy harvesting system. *Nano Energy*. 2014;8:150-156.

58. Dharmasena RDIG, Jayawardena KDGI, Mills CA, et al. Triboelectric nanogenerators: providing a fundamental framework. *Energ Environ Sci*. 2017;10(8):1801-1811.

59. Fang C, Tong T, Bu T, et al. Overview of power management for triboelectric nanogenerators. *Adv Intell Syst*. 2020;2(2):1900129.

60. Zhao Z, Dai Y, Liu D, et al. Rationally patterned electrode of direct-current triboelectric nanogenerators for ultra-high effective surface charge density. *Nat Commun*. 2020;11(1):6186.

61. Xu L, Xuan W, Chen J, et al. Fully self-powered instantaneous wireless humidity sensing system based on triboelectric nanogenerator. *Nano Energy*. 2021;83:105814.

SUPPORTING INFORMATION

Additional supporting information can be found online in the Supporting Information section at the end of this article.